SLAC-PUB-3205
LBL-16687
September 1983
(T/E)

PION PAIR PRODUCTION FROM $\gamma\gamma$ COLLISIONS AT THE SLAC e^+e^- STORAGE RING PEP*

J. R. Smith[a], D. L. Burke, A. M. Boyarski, M. Breidenbach, J. M. Dorfan, G. J. Feldman, L. Gladney, G. Hanson, R. J. Hollebeek, W. R. Innes, J. A. Jaros, A. J. Lankford, R. R. Larsen, B. LeClaire, N. Lockyer, V. Lüth, C. Matteuzzi, M. L. Perl, B. Richter, D. Schlatter[j], J. Weiss[i], J. M. Yelton and C. Zaiser
Stanford Linear Accelerator Center
Stanford University, Stanford, California 94305

G. S. Abrams, D. Amidei, W. Chinowsky, W. E. Dieterle[c], J. B. Dillon[d], M. W. Eaton[b], M. E. B. Franklin, G. Gidal, M. S. Gold, G. Goldhaber, L. J. Golding, A. D. Johnson[e], J. A. Kadyk, M. E. Nelson[f], J. F. Patrick[g], P. C. Rowson, H. M. Schellman, P. D. Sheldon, J. Strait[h] and C. de la Vaissière
Lawrence Berkeley Laboratory and Department
University of California, Berkeley, California 94720

C. A. Blocker, M. Levi[j], T. Schaad and R. F. Schwitters
Department of Physics
Harvard University, Cambridge, Massachusetts 02138

ABSTRACT

We have studied several features of the production of charged hadron pairs by $\gamma\gamma$ collisions. We have measured the f^0 partial width $\Gamma_{f^0\to\gamma\gamma}(Q^2)$ for Q in the range $0 < Q^2 < 1.4\ \mathrm{GeV}^2/\mathrm{c}^2$, and obtained $\Gamma_{f^0\to\gamma\gamma} = 2.52 \pm 0.13 \pm 0.38$ keV at $Q^2 \approx 0$. The measured Q^2 dependence is in agreement with the generalized vector dominance model. The cross section for $\gamma\gamma \to (\pi^+\pi^- + K^+K^-)$ in the mass region $1.6\ \mathrm{GeV/c^2} \leq M_{\pi\pi} \leq 2.5\ \mathrm{GeV/c^2}$ has also been measured and the result compared with that expected from the QCD continuum.

Submitted to Physical Review D

---

* This work was supported in part by the Department of Energy, contracts DE-AC03-76SF00515 (SLAC), DE-AC03-76SF00098 (LBL) and DE-AC02-76ER03064 (Harvard). Support for individuals also is from U.C. Davis, and NSF.

I. INTRODUCTION

We have studied the $\gamma\gamma$ process, $e^+e^- \rightarrow e^+e^- + 2$ charged prongs, with the MARK II detector at the e^+e^- storage ring PEP. In particular, we have measured the partial width of the $f^0(1270)$, and also measured the hadron pair production rate in the region of higher masses 1.6 GeV/c$^2 < M_{\pi\pi} <$ 2.5 GeV/c^2. When the incident beam leptons are not observed in the final state the event is said to be ***untagged*** and both of the photons involved have negligible Q^2. A measurement of the untagged production cross section $\sigma(\gamma\gamma \rightarrow f^0)$ provides a value for $\Gamma_{f^0\rightarrow\gamma\gamma}$ at $Q^2 \approx 0$. Events in which one of the outgoing beam leptons is detected are said to be ***single tagged*** and provide a measurement of the Q^2 dependence of the production cross section. We have studied both single tagged and untagged production of the $f^0(1270)$ and have made comparisons of our results with various theoretical models. Perturbative QCD predictions[1] have been made for the $\gamma\gamma \rightarrow \pi^+\pi^-$ and $\gamma\gamma \rightarrow K^+K^-$ processes at high invariant mass, and we compare these with our measurements of untagged hadron pairs with $M_{\pi\pi} >$ 1.6 GeV/c^2.

Production of the $f^0(1270)$ by two real ($Q^2 \approx 0$) photons has been studied by many groups, including the MARK II at SPEAR, the Crystal Ball at SPEAR, and the TASSO, PLUTO, JADE, and CELLO Collaborations at PETRA. The value of the partial width $\Gamma_{f^0\rightarrow\gamma\gamma}$ found in the latest Particle Data Group tables[2] is 2.86 ± 0.05 keV. The TASSO[3] collaboration has measured the production of the f^0 in the tagged mode with $Q \approx 0.35$ GeV^2/c^2 and has found that the partial width, extrapolated to $Q^2 = 0$ with a form factor given by Ref. 4, is $1.6 \pm 0.6 \pm 0.3$ keV, which is smaller than the value of $\Gamma_{f^0\rightarrow\gamma\gamma}$ that they report for the untagged case. The PLUTO[5] collaboration has placed an upper limit $\Gamma_{f^0\rightarrow\gamma\gamma} < 2.6$ keV for a range of Q^2 similar to the TASSO range. A measurement of the double-tagged production of the f^0 made at SPEAR[6] obtained a partial width of $9.5 \pm 3.9 \pm 2.4$ keV for Q^2 values of each virtual photon in the range

$0.07 - 0.3\ \mathrm{GeV}^2/c^2$. Measurements of the cross section for $\gamma\gamma \to (\pi^+\pi^- + K^+K^-)$ at masses below $\approx 1.5\ \mathrm{GeV}/c^2$ have been made by the MARK II group at SPEAR.[7] The cross section in this mass region was found to be consistent with that expected from the Born amplitude for point-like pions and the $f^0(1270)$ meson. In this paper we report measurements of $\sigma(\gamma\gamma \to \pi^+\pi^-) + \sigma(\gamma\gamma \to K^+K^-)$ at masses above the $f^0(1270)$ and make comparisons with predictions from perturbative QCD calculations.

In the following sections we discuss the results of the present measurements. The first section contains a brief description of the central part of the MARK II detector. The second section describes the apparatus used to detect electrons scattered at small angles with respect to the beam direction. In the third and fourth sections we present discussions of the untagged and tagged data respectively.

II. CENTRAL DETECTOR

The MARK II central detector, shown in Fig. 1, has been previously described in detail.[8,9] Charged particle tracking is accomplished with multilayer cylindrical drift chambers centered in a 2.3 kG solenoidal magnet. The momentum resolution of the spectrometer is $\Delta p/p = \sqrt{(0.02) + (0.0095p)^2}$ (p in GeV/c) for tracks constrained to the beam intersection point (IP). This momentum resolution is more than sufficient for the purpose of the work presented in this paper. The minimum momentum required for a particle to traverse all of the drift chamber layers is 100 MeV/c, and the detector is triggered on events that have at least two particles with momentum greater than this value and angles to the beam direction (θ) greater than 45°. The momentum cut-off causes no problem for the detection of the f^0, since the momentum distribution for the $\pi^+\pi^-$ from the decay of the f^0 peaks around 600 MeV/c, and the probability that an individual pion has a momentum less than 100 MeV/c from such a decay is very small (less than 0.2%). A time of flight system (TOF), consisting of scintillation counters at a radius of 1.5m, measures flight times with a resolution of ~ 320 psec for particles with $|\cos\theta| < 0.76$. The TOF system is part of the charged particle trigger and is also used to reject cosmic rays and identify protons below a momenta of 2 GeV/c. Electromagnetic showers are identified with an energy resolution of $\sigma_E \simeq 14\% \sqrt{E}$ (energy in GeV) using eight lead-liquid argon (LA) calorimeter modules. The LA system covers the region $|\cos\theta| < 0.7$ and is used to separate electrons from hadrons at momenta above 600 MeV/c. Muons of momenta ≥ 750 MeV/c are identified over 55% of 4π steradians with four layers of iron absorber interleaved with proportional tubes.

III. SMALL ANGLE TAGGER

One arm of the small angle tagging (SAT) system is shown in Fig. 2. A detailed description of this hardware can be found in Ref. 10; here we give a brief sketch of the apparatus. It consists of three sets of four planar drift chambers and a pair of electromagnetic shower counters. These drift chambers and shower counters cover the polar angles between 21 mr and 82 mr from the beam axis. It would also be possible to tag electrons in the central detector (20° to 160°), but the rate is too low to be useful for the present study of the f^0.

Each plane of drift chambers is arranged around the beam pipe in a rectangular array with two vertical chambers and two horizontal chambers. The spatial resolutions of these chambers is $\approx 300\ \mu$m in the drift coordinate, and a delay line under each sense wire provides a measurement of the orthogonal coordinate with a resolution of $\approx$ 0.5 cm. In the region of overlap (i.e., the corners), one obtains good resolution in both the x and y coordinates which are orthogonal to the beam direction. The accuracy of the measurement of the track's slope and intercept depends on the number of x and y hits made by the track in the drift chambers and also on random noise hits assigned to the track. Each reconstructed track was projected backward along the beamline to the x-y plane at the z position of the IP, and all tracks that project radially to within

3 cm of the IP were used in the analysis presented here. Since well-measured tracks are more likely to have a small intercept at the IP x-y plane than poorly measured tracks, the acceptance in the regions where the x and y chambers overlap is better than in the non-overlap region where only one coordinate is measured well. The efficiency in the overlapping sections of the chambers was determined to be $96 \pm 0.5\%$ from a study of Bhabha events and checked with a Monte Carlo simulation that used the EGS electromagnetic shower code.[11] The efficiency in the non-overlapping sections was determined to be $58 \pm 5\%$ by taking the ratio of the accepted events in the non-overlapping sections to those in the corners, suitably correcting for the difference in solid angle, and then multiplying by the measured efficiency in the corners.

The electromagnetic shower counter modules are constructed of sandwiches of 0.63 cm lead sheets and 1.27 cm NE114 plastic scintillators. There are eighteen layers each of lead and scintillator. Waveshifter bars (BBQ) are used to transmit light from the scintillators to standard 44 mm photomultiplier tubes. The energy resolution of these shower counters was measured with Bhabha events and found to be $\sigma_E = 15.5\% \cdot \sqrt{E}$. The first five layers of the shower counter are read out together and the last thirteen layers are read out together.

IV. RESULTS FROM THE UNTAGGED DATA

For the untagged data, we demanded that just two charged prongs with opposite charges be found in the central detector. The detected pair was required to form a vertex with position coordinate along the beam axis within 6 cm of the IP, and radial distance from the beam axis less than 3 cm. Each prong was required to be within the region $|\cos\theta| < 0.7$ to eliminate uncertainties in the acceptance of the trigger logic. Cosmic ray events were rejected by time of flight measurements. Protons and pions with momenta $p \leq 1$ GeV/c are well separated by time of flight and so events with either prong identified as a proton were removed. Since the momenta of the pions from the f^0 are typically around 600 MeV/c, the muon system was not used, and electron separation with the liquid argon system was not attempted because of the rapidly varying electron detection efficiency in this region. To eliminate beam gas background and also contamination from higher multiplicity states the total transverse momentum of the pair was required to be less than 100 MeV/c. This requirement effectively limits the Q^2 of the accepted events to less than 0.04 GeV^2/c^2. Figure 3 shows the mass plot obtained with these selection criteria from an integrated luminosity of 14.5pb^{-1} at a beam energy of 14.5 GeV. All the prongs were assumed to be pions. This two-prong sample is dominated by the QED processes $e^+e^- \to e^+e^-e^+e^-$ and $e^+e^- \to e^+e^-\mu^+\mu^-$. However, one can distinctly see the f^0 resonance in the data.

Data from SPEAR[7] indicate that, in addition to the f^0, there is non-resonant pion production in the mass region shown in Fig. 3. This non-resonant pion contribution can interfere with the resonant pion component. A fit to the data in Fig. 3 was performed using a Monte Carlo calculation of the QED mass shape[12] and also a model for the pion mass spectrum. This model allows for interference between the f^0 resonance and the continuum by using a relative phase shift between the two channels given by the angle δ where:

$$\tan\delta(M_{\pi\pi}) = \frac{M_{f^o}\Gamma_{\rm tot}}{M_{f^o}^2 - M_{\pi\pi}^2} \quad .$$

The pion cross section was assumed to have the form:[7]

$$\begin{aligned} \frac{d\sigma}{d\Omega^*}(\gamma\gamma \to \pi\pi) = A \cdot h(M_{\pi\pi}) + \Gamma_{f^0\to\gamma\gamma} \cdot g(M_{\pi\pi}) + \; f'(M_{KK} \to M_{\pi\pi}) \\ + \; 2 \cdot B \cdot \cos\delta(M_{\pi\pi}) \cdot \sqrt{\Gamma_{f^0\to\gamma\gamma} A\, h(M_{\pi\pi})\, g(M_{\pi\pi})} \quad . \end{aligned} \tag{1}$$

Here $h(M_{\pi\pi})$ represents the pion continuum mass shape which was chosen to be a combination of the Born cross section and the QCD cross section.[1] The Born term was assumed to be valid for $M_{\pi\pi}$ below 1 GeV/c^2 and QCD valid for $M_{\pi\pi}$ above 1

GeV/c^2. These are approximately equal at $M_{\pi\pi} = 1\,\mathrm{GeV}/c^2$, so the normalization of the QCD shape was adjusted to make them equal at 1 GeV/c^2 and the parameter A was then used in the fit described below. The function $g(M_{\pi\pi})$ contains the relativistic Breit-Wigner line shape of the f^0 and also the assumed helicity-2 angular distribution. It is given by:

$$g(M_{\pi\pi}) = \frac{8\pi^2(2J+1)}{M_{\pi\pi}} \cdot |Y_{22}|^2 \cdot \frac{1}{\pi} \cdot \frac{M_{f^o}\Gamma_{\mathrm{tot}}}{(M_{\pi\pi}^2 - M_{f^o}^2)^2 + M_{f^o}^2\Gamma_{\mathrm{tot}}^2} \cdot BR_{f^o\to\pi^+\pi^-} \quad . \tag{2}$$

Here Γ_{tot} is the effective resonance total width which has mass dependence due to the centrifugal potential:[13]

$$\Gamma_{\mathrm{tot}}(M_{\pi\pi}^2) = \Gamma_{f^o} \cdot \left(\frac{q(M_{\pi\pi}^2)}{q(M_{f^o}^2)}\right)^{2J+1} \cdot \frac{D_2(q(M_{\pi\pi}^2)\cdot r_{f^o})}{D_2(q(M_{f^o}^2)\cdot r_{f^o})} \quad , \tag{3}$$

where $q(s) = \sqrt{s/4 - m_\pi^2}$ and $D_2(z) = (9 + 3z^2 + z^4)^{-1}$. In the above we have taken the following constants appropriate for the f^0 meson:

$$\begin{aligned} J &= 2 \quad , \\ r_{f^o} &= 1 \text{ fermi } = 5.068(\mathrm{GeV}/c)^{-1} \quad , \\ \Gamma_{f^o} &= 0.180\,\mathrm{GeV} \quad , \\ M_{f^o} &= 1.270\ \mathrm{GeV}/c^2 \quad , \end{aligned}$$

and

$$BR_{f^o\to\pi^+\pi^-} = \frac{2}{3} \cdot 0.831 \quad .$$

A partial wave decomposition was not attempted and therefore a parameter B was inserted into the fit. If the continuum and the resonance were in the same partial wave B would be 1. Since kaons were not explicitly eliminated, the two-prong data sample can also contain $f'(1515)$ decays. To correct for this we include a fixed contribution from $f' \to K^+K^-$ using the partial width[14] $\Gamma_{f'\to\gamma\gamma} = 0.11$ keV . The f^0

produced in the untagged case is known to be predominantly produced in helicity-2.[15] By assuming that the cross section for $e^+e^- \to e^+e^-\pi^+\pi^-$ factorizes into a $\gamma\gamma$ cross section multiplied by a $\gamma\gamma$ luminosity function, we can write in the untagged case:[16]

$$\frac{d\sigma(ee \to ee\pi^+\pi^-)}{dM\,d\Omega^*} = \left[\frac{2\alpha}{\pi}\log\frac{E_{beam}}{m_e}\right]^2 \frac{f(z)}{M}\,\frac{d\sigma(\gamma\gamma \to \pi^+\pi^-)}{d\Omega^*} \tag{4}$$

where M is the $\pi^+\pi^-$ invariant mass and $z = M/2E_{beam}$. The function $f(z)$ is the photon flux density. For untagged processes it is approximately:[17]

$$f(z) = (2+z^2)^2 \log\frac{1}{z} - (1-z^2)(3+z^2) \quad . \tag{5}$$

The actual formula that we used was taken from a more precise formulation[18] that accounts for the small Q^2 spread of the untagged events. The above model, with $\Gamma_{f^0\to\gamma\gamma}$ used as a parameter, was fitted to the data. The normalization of the QED contribution was also allowed to be a free parameter of the fit. The partial width was stepped through a series of values and the remaining parameters varied to minimize the χ^2 at each value of $\Gamma_{f^0\to\gamma\gamma}$. The overall minimum χ^2 was found to give $\Gamma_{f^0\to\gamma\gamma} = 2.52 \pm 0.13$ keV . At this minimum the normalization of the QED was 92% of that obtained from the measured luminosity, but the equivalent photon approximaton used to compute[16] the QED mass shape is known to overestimate the absolute cross section by 10-20%. The fit also gave $B = 0.93$. Because of the detector acceptance most of the observed Born cross section is in helicity 2 and so B very near to 1 is a reasonable value. Such a large interference also accounts for approximately half of the 50 MeV shift of the observed mass peak relative to the nominal f^0 mass. The falling photon flux explains the remainder of the observed shift. The value of $\Gamma_{f^0\to\gamma\gamma}$ from the fit can be compared with the result of a more approximate analysis in which a straight subtraction of the sidebands was performed using a smooth curve obtained by renormalizing the QED mass shape in the mass region 0.6 GeV/c^2 to 0.9 GeV/c^2. This method gives a value for the partial width of $\Gamma_{f^0\to\gamma\gamma} = 2.68 \pm 0.13$ keV in close agreement with the value obtained from the fit.

The errors quoted above are only the statistical uncertainty of the experiment. The major components of the systematic error are the accuracy of the Monte Carlo calculation of the acceptance of the detector and uncertainties in the $\gamma\gamma$ process itself. We have assumed that the $f(1270)$ is produced in the helicity-2 state. There is evidence from the Crystal Ball[15] that this is the case; however, the detector efficiency for the helicity-0 case is approximately half of that for the helicity-2 final state. We also must correct the measured value for the efficiency of the cut at 100 MeV/c on the total transverse momentum of the detected pair. This was done by using Monte Carlo distributions for the $\gamma\gamma$ cms motion that are consistent with exact calculations[12] for the QED process $ee \to ee\mu\mu$. This, however, assumes that the Q^2 dependence of the production of the f^0 is the same as that for QED (see next section). The accumulated luminosity of the experiment is known to $\pm 3\%$. By assuming these to be uncorrelated errors and adding them in quadrature, we estimate the total systematic error to be 15%. Therefore the value of the partial width we measure is $\Gamma_{f^0\to\gamma\gamma} = 2.52 \pm 0.13 \pm 0.38$ keV. This value can be compared with the MARK II SPEAR value of $3.6\pm0.3\pm0.5$ keV.

Figure 4 shows measured values reported in the literature[19] for the partial widths of the 2^{++} tensor mesons with our new value also shown. Using ideal mixing, this multiplet has the quark assignments $f = (u\bar{u} + d\bar{d})/\sqrt{2}$, $A_2 = (u\bar{u} - d\bar{d})/\sqrt{2}$, and $f' = (s\bar{s})$. SU(3) symmetry predicts that the $\gamma\gamma$ partial widths of these resonances should be in the ratio of 25:9:2. This SU(3) prediction is shown by the dashed arrows in Fig. 4 using the average value of the f^0 partial width as input and corrected for the different phase space due to the shift in mass of the f' (an m^3 correction was assumed) relative to the other members of this multiplet. The mass splitting itself is evidence that the SU(3) symmetry is only approximate. However, in view of the uncertainty regarding the helicity structure of these reactions, the SU(3) prediction of the partial widths is reasonably close to the data.

Equation (1) can be checked in an independent way. It makes a prediction for the pion cross section for masses above the f^0 resonance. In this region the liquid argon and muon system can be used to reject the QED background, thus allowing a direct measurement of cross section $\sigma(\gamma\gamma \rightarrow$ hadron pairs). We have measured $\sigma(\gamma\gamma \rightarrow$ hadron pairs) in the mass region 1.6 GeV/c$^2 \leq M_{\pi\pi} \leq$ 2.5 GeV/c^2. We demanded $|\cos\theta| < 0.56$ for both tracks, effectively limiting $|\cos\theta^*|$ to be between 0 and 0.3 (θ^* is the angle between the $\gamma\gamma$ axis and the angle of emission of the hadron pair in the $\gamma\gamma$ center of mass system). Therefore we present the cross section integrated over the region $|\cos\theta^*_\pi| < 0.3$. The data sample used for this measurement corresponds to an integrated luminosity of 35 pb^{-1}.

The liquid argon modules measured the shower energy, E_{sh}, deposited by each prong. Prongs with E_{sh}/p greater than 0.5 were identified as electrons, and events with either track identified as an electron were removed. Events were also removed if either track fell within $\pm 2°$ of a crack between any two of the eight liquid argon modules. The scatter plot shown in Fig. 5 of E_{sh}/p for one prong versus the other for all two-prong events shows a clean separation between e^+e^- pairs and the remainder of the two-prong sample. From this plot we estimate the probability that both electrons in an e^+e^- pair have E_{sh}/p less than 0.5 to be 0.02%. The muon system was used to reject μ-pairs. We checked different ways of cutting on the response of the muon system, and found that the final measured cross sections were not extremely sensitive to the choice of cuts. The first technique was to require that each charged track penetrate fewer layers of steel than would be expected if it were a muon. The second technique was to require that only one charged track have penetrated fewer layers of steel than would be expected for a muon and the other track was not identified as a muon. This accepts some events in which one track falls into the gaps in the azimuthal coverage of the muon system. In the third technique the analysis was carried out with the more stringent requirement that at least one prong have not penetrated any layers of the muon system while the other prong simply failed to be identified as a muon. Here, as in the second technique, some events are accepted with one prong falling into the azimuthal gaps in the muon system. The data sample with electrons removed was used to make an estimate of the number of μ-pair events that are misidentified as hadron pairs by these techniques. Events with one prong identified as a muon were used to determine the probablity that the partner is misidentified as a hadron. We find that the misidentification probablity for μ-pairs is $\approx 0.3\%$ for the first technique, $\approx 1.4\%$ for the second technique, and $\approx 0.3\%$ for the third technique of muon identification. These misidentification probabilities are essentially independent of mass in the region of interest.

The efficiency for pion events to be accepted by the above analysis was computed by Monte Carlo, and was found to be 9.5% for the first and third muon identification techniques and 11.5% for the second technique. In the mass region 1.6 GeV/c^2 to 2.5 GeV/c^2 we find 41 events that survive the cuts of the first muon identification technique, 59 events using the second technique, and 43 using the third technique. The estimated QED background was subtracted bin-by-bin in the $\pi\pi$ invariant mass to yield the $\gamma\gamma$ cross section shown in Fig. 6. This subtraction ranged from $\approx 10\%$ at 1.6 GeV/c^2 to $\approx 50\%$ at 2.5 GeV/c^2. The errors shown in the plot include contributions from the uncertainties in the photon flux and pion pair acceptance, and from the uncertainty in the background subtraction. This latter uncertainty has been estimated from the spread in the results obtained from the different identification techniques described above. Also shown in Fig. 6 is the absolute prediction of a perturbative QCD calculation[1] for pions and kaons with pion masses used throughout. The comparison of the cross section with the QCD prediction indicates agreement in the high mass region, although the data are statistically limited in this region.

V. RESULTS FROM THE TAGGED DATA

Events with two oppositely charged prongs in the central detector were examined to see if there was a beam lepton detected by the SAT system. Events were kept if a track in the SAT system projected back to within 3 cm of the origin defined by the vertex formed by the charged prongs in the central detector. It was required that the z position of the vertex formed by the two prongs in the central detector be within 7 cm of the IP and the radial distance of this vertex from the beam axis was required to be less than 3.5 cm. As in the untagged case, each of the charged prongs in the central detector region was required to be between 45° and 135° from the beam axis. To isolate tagged $\gamma\gamma \rightarrow 2$ prong events from higher multiplicity final states we examined the transverse momentum balance between the tagged electron and the two prongs seen in the central detector. Events with net transverse momentum less than 200 MeV/c were kept. Figure 7 shows a scatterplot of energy of the tagged electron versus the total visible transverse momentum of the event before the cuts. The tagged energy distribution from $\gamma\gamma$ events peaks near the beam energy and has a long tail extending into the lower energy region. Below 2 GeV the population rises due to background tracks ($\approx 10\%$ occupancy). Events with tagged electron energy greater than 8 GeV were kept. Also, since Monte Carlo studies indicate that the efficiency for detecting an f^0 falls off rapidly for $|\cos\theta^*_\pi| > 0.8$, events in this range were rejected.

The tagged data were divided into two regions of Q^2. The first region has Q^2 values extending from 0.05 GeV^2/c^2 to 0.26 GeV^2/c^2 and the second region from 0.26 GeV^2/c^2 to 1.4 GeV^2/c^2. The resulting mass plots are shown in Figure 8. The transverse-transverse part of the $\gamma^*\gamma$ cross section, valid for single tagging, is given by:[18,20]

$$\frac{d^5\sigma}{d\omega_1\, d\omega_2\, d\theta_{tag}\, d\Omega^*} = \frac{d^3\mathcal{L}_{TT}(Q^2)}{d\omega_1\, d\omega_2\, d\theta_{tag}}\ \frac{d^2\sigma_{TT}(Q^2)}{d\Omega^*}\ (\gamma\gamma \to \pi^+\pi^-) \quad . \tag{6}$$

Here ω_1 and ω_2 are the untagged and tagged photon total energies respectively, divided by the beam energy, while θ_{tag} is the angle of the tagged electron. Also, Ω^* is the center of mass solid angle element of the pion pair. Experimentally one measures the cross section for $e^+e^- \to e^+e^- + 2$ charged prongs. Equation (6) then forms the basis for converting this cross section into a measurement of the cross section for $\gamma\gamma \to 2$ charged prongs at non-zero Q^2. The photon luminosity function, $\mathcal{L}_{TT}$, is given by:

$$\begin{aligned} \frac{d^3\mathcal{L}_{TT}}{d\omega_1\, d\omega_2\, d\theta_{tag}} \approx \frac{\alpha^2}{8\pi^2} K \cot\left(\frac{\theta_{tag}}{2}\right)\left[\frac{(K-2\omega_1)^2}{K^2}+1\right] \times \\ \left[\left(\frac{(K-2(\omega_2+Q_2^2)^2}{K^2}+1\right) \log\left(\frac{2E_b(1-\omega_1)}{m_e\omega_1}\sin\frac{\hat{\theta}}{2}\right)\right. \\ \left. -\frac{2(1-\omega_1)}{\omega_1^2}+\frac{m_e^2}{2E_b^2(1-\omega_1)\sin^2(\hat{\theta}/2)}\right], \end{aligned} \tag{7}$$

where E_b is the beam energy and $K = (M_{\pi\pi}^2 + Q^2)/4E_b^2$. Also $\hat{\theta}$ is the minimum tagging angle which is the upper limit in the integration over the untagged electron's polar angle. We have explicitly removed events from our data sample in which <u>both</u> beam electrons are detected in the SAT system. In writing expression (6) we have assumed that the Q^2 dependence of the cross section factors into a part that describes the massive photon propagator, $\mathcal{L}_{TT}(Q^2)$, and a part that describes the coupling of the photon to the final state, $d\sigma(Q^2)/d\Omega^*$.

Just as in the untagged case we fit the mass distributions with a QED component and a pion continuum that is allowed to interfere with the resonant $f^0(1270)$. In Fig. 9 we show the Q^2 distribution of the data and compare it with a Monte Carlo calculation[12] of the expected shape for QED processes. We have simply used all events in this figure since the QED completely dominates the mass spectrum. The results of the fits to the two regions of Q^2 are shown in Fig. 8. The total integrated luminosity used for this analysis was also 35 pb^{-1}. The results yield a value of the partial width of $1.92 \pm 0.32 \pm 0.39$ keV for $Q^2 < 0.26$ GeV^2/c^2 and of $1.25 \pm 0.28 \pm 0.27$ keV for $0.26 < Q^2 < 1.4$ GeV^2/c^2. We did not measure the center-of-mass angular dependence of the f^0 decay and hence made the assumption for this analysis that it is in the helicity-2 state, just as in the untagged case. Hence, the efficiency for detection of the $\pi^+\pi^-$ pair from the f^0 was determined using angular distributions appropriate for the helicity-2 hypothesis. The major systematic errors are uncertainties in the Monte Carlo calculation of the tagged electron track reconstruction efficiencies, the net transverse momentum distribution of the $\gamma\gamma$ cms, and the acceptance of the detector. These are each approximately 10%. Also, the uncertainty in the tagged energy distribution and the modeling of the central detector contribute approximately 5% each to the systematic error. Assuming these to be uncorrelated errors and adding them in quadrature gives a resultant systematic error of approximately 20%. The QED normalization from the fits was 93% for $Q^2 < 0.26$ GeV^2/c^2 and 108% for $0.26 < Q^2 < 1.4$ GeV^2/c^2 of that expected from the measured luminosity and our Monte Carlo program.

The values quoted above for the partial width can be compared with approximate results obtained by using the QED mass shape as a smooth curve through the background. This method entails renormalizing the QED mass shape in the region between 600 and 900 MeV/c^2 and subtracting the renormalized QED component in the mass region 1000 to 1500 MeV/c^2. The results of this subtraction technique yield a signal of 236 ± 35 events in the data with $Q^2 < 0.26$ GeV^2/c^2 and 188 ± 35 events in the data with 0.26 GeV^2/c^2 $<$ Q^2 $<$ 1.4 GeV^2/c^2. Attributing all of the events in the signal to the f^o gives partial widths $\Gamma_{f^o \to \gamma\gamma} = 2.0 \pm 0.3$ keV for $Q^2 < 0.26$ GeV^2/c^2 and $\Gamma_{f^o \to \gamma\gamma} = 1.2 \pm 0.2$ keV for $0.26 < Q^2 < 1.4$ GeV^2/c^2. The values of the partial width obtained for the three regions of Q^2 are summarized in Fig. 10. The errors shown in this figure include the statistical uncertainties as well as systematic errors which are not common to the tagged and untagged analyses.

Vector meson dominance has historically been used to describe the interaction of off-mass shell photons. One generalized vector dominance model[21] (GVDM) predicts a shape given by the solid curve in Fig. 10. This curve is normalized to the world average value of 2.8 keV at $Q^2 = 0$. Basically this model includes contributions from the ρ, ω and ϕ mesons as well as higher resonances and a continuum. Also included in this GVDM are contributions from the longitudinal-transverse photon combinations. The dot-dashed curve is the ρ form factor alone normalized to the same $Q^2 = 0$ value. The data tend to prefer the less rapid decrease in Q^2 given by the GVDM of Ref. 21.

An explanation of the data can also be attempted in the framework of the quark model. The nonrelativistic quark model has been used[4] to calculate the Q^2 dependence of the $\gamma^*\gamma f^0$ vertex. The bound state problem was treated using a Bethe–Salpeter amplitude for the quark–anti-quark amplitude. Essentially an effective "form factor" is calculated from the Bethe–Salpeter amplitude which provides an enhancement over the ρ form factor of about 20% for tagging angles between 24 mr and 60 mr. This effective form factor is closer to our result than the ρ form factor. Relativistic calculations[22] are being performed to improve this model.

In all of the above data analysis, we have assumed that the f^0 is produced in the helicity-2 state. The parton model predicts[23] that, as $Q^2 \to \infty$, only the helicity-0 amplitude will remain because two photons with spins aligned cannot couple to a quark–anti-quark pair in the approximation that the quark mass is zero. This is because the helicity-changing part of the quark current is proportional to the quark mass. Hence, we might expect that there will be a rapid change in the angular distribution as Q^2 is increased from 0 to the asymptotic region (i.e., where scaling sets in).

Unfortunately, the region in between is a mixture of helicity states, and the parton model does not provide a clear description. There was not enough data to perform a detailed study of the angular dependence of the production process as a function of Q^2. The efficiency for detecting an helicity-2 f^0 in the tagged data is approximately twice as large as that for an helicity-0 tagged f^0 event. If we assume that at $Q^2 = 0$ the f^0 is produced purely in helicity-2 and that at $Q^2 = 0.6$ GeV^2/c^2 the f^0 is produced purely in helicity-0, the difference in detection efficiency is a viable explanation of the data without any furthur suppression. We would obtain a partial width of $\Gamma_{f^0 \to \gamma\gamma} =$ 1.26 keV at $Q^2 = 0.6$ GeV^2/c^2 (i.e., our data are consistent with a transition from helicity-2 at $Q^2 = 0$ to helicity-0 at $Q^2 = 0.6$ GeV^2/c^2).

VI. CONCLUSION

We have measured the coupling of the $f^o(1270)$ meson to two real photons and find a partial width $\Gamma_{f^o \to \gamma\gamma}$ that is consistent with previous measurements. In addition we have studied the Q^2 dependence of $\Gamma_{f^o \to \gamma\gamma}(Q^2)$ and find that it is consistent with a generalized vector dominance model form factor.[21] The data can also be explained by the nonrelativistic quark model.[4] In addition the production of 2 prong hadron states via the $\gamma\gamma$ interaction is in reasonable agreement with QCD predictions[1] for $\gamma\gamma$ masses $\gtrsim 2.0$ GeV/c^2.

Acknowledgement

We gratefully acknowledge many enlightening discussions with S.J. Brodsky on topics relevant to this work.

References

[a] University of California, Davis, California 95616.

[b] Present address: Harvard University, Cambridge, Massachusetts 02138.

[c] Present address: University of Arizona, Tucson, Arizona 85721.

[d] Present address: Xerox Corp., Palo Alto, California.

[e] Present address: University of California at Santa Cruz, Santa Cruz, California 95064.

[f] Present address: California Institute of Technology, Pasadena, California 91125.

[g] Present address: Fermilab, Batavia, Illinois 60510.

[h] Present address: University of Massachusetts, Amherst, Massachusetts 01002.

[i] Present address: Argonne National Laboratory, Argonne, Illinois 60439.

[j] Present address: CERN CH-1211 Geneva 23, Switzerland.

1. S.J. Brodsky and G.P. Lepage, *Physical Review D* 24, 1808 (1981); and S.J. Brodsky and G.P. Lepage, SLAC-PUB-2762 (1981), also published in the Proceedings of the Tallahasse Conference (1981), p.214; and S.J. Brodsky and G.P. Lepage, *Physical Review D* 22, 2157 (1980).
2. The Partical Data Group, *Physics Letters* 111B (April 1982).
3. R. Brandelik *et al.,* TASSO Collaboration, *Zeitschrift für Phys. C* 10, 117 (1981).
4. H. Krasemann and J.A.M. Vermaseren, *Nuclear Physics* B184, 269 (1981).
5. E. Hilger, BONN-HE Print-81-4 (1981).
6. C.J. Biddick *et al., Physics Letters* 97B, 320 (1980).
7. A. Roussarie *et al., Physics Letters* 105B, 304 (1981).
8. R. Schindler, Ph.D. Thesis, SLAC–PUB–265 (1980).

9. J.A. Jaros, in Proceedings of the International Conference on Instrumentation for Colliding Beam Physics, Stanford, California, 1981, edited by W. Ash, Stanford Linear Accelerator Report No. 250 (1982), p. 29 (unpublished).

10. J.R. Smith, Ph.D. Thesis, U. C. Davis, Dec 1982.

11. R.L. Ford and W.R. Nelson , SLAC–PUB–2107 (1978).

12. The Monte Carlo used only the σ_{TT} part of the QED cross section [Budnev, *et al., Physics Reports* 15, 181 (1975)]. The QED mass shape is also in agreement with the Smith-Vermaseren Monte Carlo program. J. Smith, J.A.M. Vermaseren and G. Grammer, *Physical Review D* 15, 3280 (1977).

13. J.M. Blatt and V.F. Weisskopf, *Theoretical Nuclear Physics,* Wiley Publication (New York: John Wiley and Sons, 1952) pp. 359–365 and pp. 386–389, we have used equation (7.13) for Γ_{tot} normalized to the value 180 MeV at $M = 1.27$ GeV/c^2.

14. M. Althoff *et al.,* TASSO Collaboration, *Physics Letters* 121B, 216 (1983).

15. C. Edwards *et al., Physics Letters* 110B, 82 (1982).

16. S. J. Brodsky, T. Kinoshita and H. Terazawa *Physical Review D*, 1532 (1971).

17. F.E. Low, *Physical Review* 120, 582 (1960).

18. G. Bonneau, M. Gourdin and F. Martin, *Nuclear Physics* B54, 573 (1973).

19. D.L. Burke, SLAC-PUB-2988 (1982), *Journal de Physique*, C3, 513 (December 1982).

20. J.H. Field, *Nuclear Physics* B168, 477 (1980).

21. I.F. Ginzburg and V.G. Serbo, *Physics Letters* 109B, 231 (1982).

22. L. Bergström, G. Hulth and H. Snellman, REF. TH. 3381–CERN (1982).

23. G. Köpp, T.F. Walsh and P. Zerwas, *Nuclear Physics* B70, 461 (1974).

Figure Captions

Fig. 1. Isometric view of the MARK II central detector.

Fig. 2. The Small Angle Tagging system.

Fig. 3. Observed untagged $\gamma\gamma \rightarrow$ 2 prong mass spectrum (14.5 pb^{-1}). The curve is the result of a fit described in the text. The insert shows the result of the fit on a linear scale in the mass region around the f^0.

Fig. 4. Summary of measured partial widths of the 2^{++} tensor mesons. Only the reported statistical errors of the measurements are shown. Dashed arrows indicate the phase-space corrected SU(3) predictions for $\Gamma_{f' \rightarrow \gamma\gamma}$ and $\Gamma_{A_2 \rightarrow \gamma\gamma}$ using the average experimental value of $\Gamma_{f^o \rightarrow \gamma\gamma}$ as input.

Fig. 5. Scatterplot of the ratio of shower counter energy to momentum for one prong versus the other in untagged high-mass events.

Fig. 6. Measured cross section for $\gamma\gamma \rightarrow \pi^+\pi^-$ plus $\gamma\gamma \rightarrow K^+K^-$ integrated over the angular region $|\cos\theta^*| < 0.3$. The errors contain systematic as well as statistical contributions. The curve is a perturbative QCD prediction.

Fig. 7. Scatterplot of tag energy versus net transverse momentum in observed events. The box shows the region in which events were accepted as tagged two-photon events.

Fig. 8. Single tagged $\gamma\gamma \rightarrow$ 2 prong mass spectrum for $0 < Q^2 < 0.26$ GeV^2/c^2 and for $0.26 < Q^2 < 1.4$ GeV^2/c^2.

Fig. 9. The Q^2 distribution of the tagged 2-prong events compared with a Monte Carlo calculation of the Q^2 dependence of the purely QED processes $ee \rightarrow eeee$ and $ee \rightarrow ee\mu\mu$.

Fig. 10. Measured $\gamma\gamma$ partial width of the $f^0(1270)$ for three bins in Q^2. The resonance was assumed to be produced in the helicity-2 state in all three cases. The errors shown do not include systematic contributions common to the three parts. The solid curve is a generalized vector meson dominance form factor. The dot-dashed curve is a simple ρ-form factor. These predictions have been normalized at $Q^2 = 0$ to the value quoted in the Particle Data Group tables.

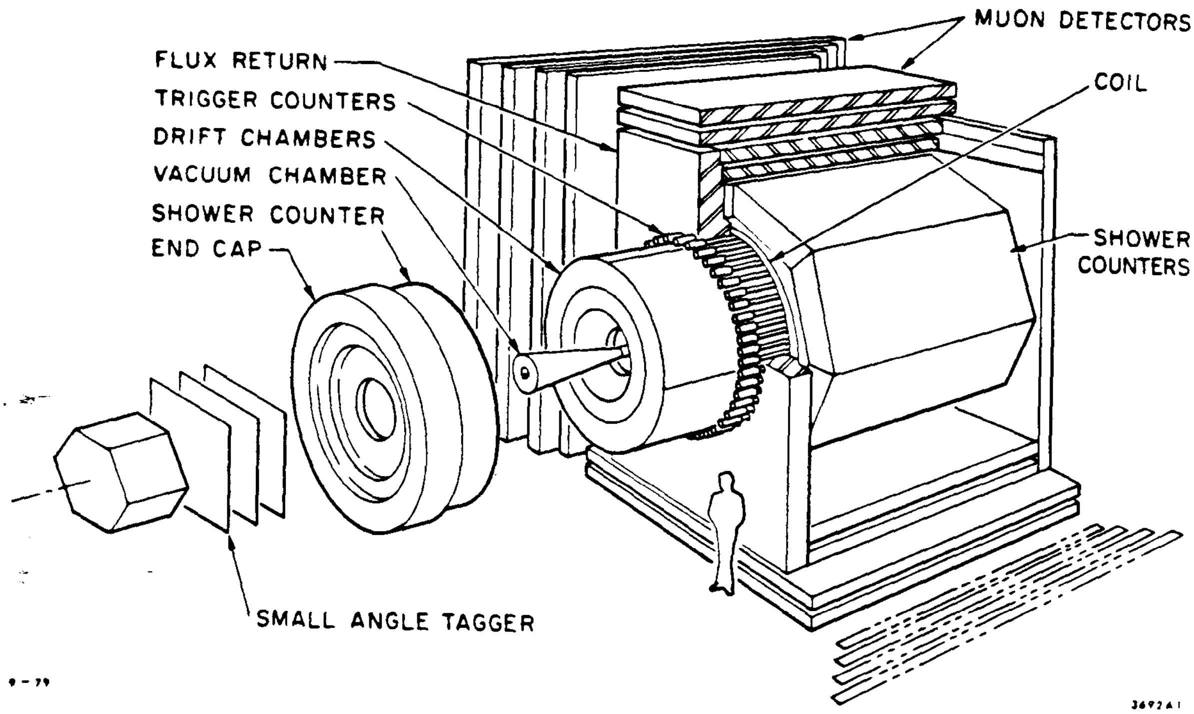
MUON DETECTORS
FLUX RETURN
COIL
TRIGGER COUNTERS
DRIFT CHAMBERS
VACUUM CHAMBER
SHOWER COUNTER
END CAP
SHOWER
COUNTERS
SMALL ANGLE TAGGER

Fig. 1

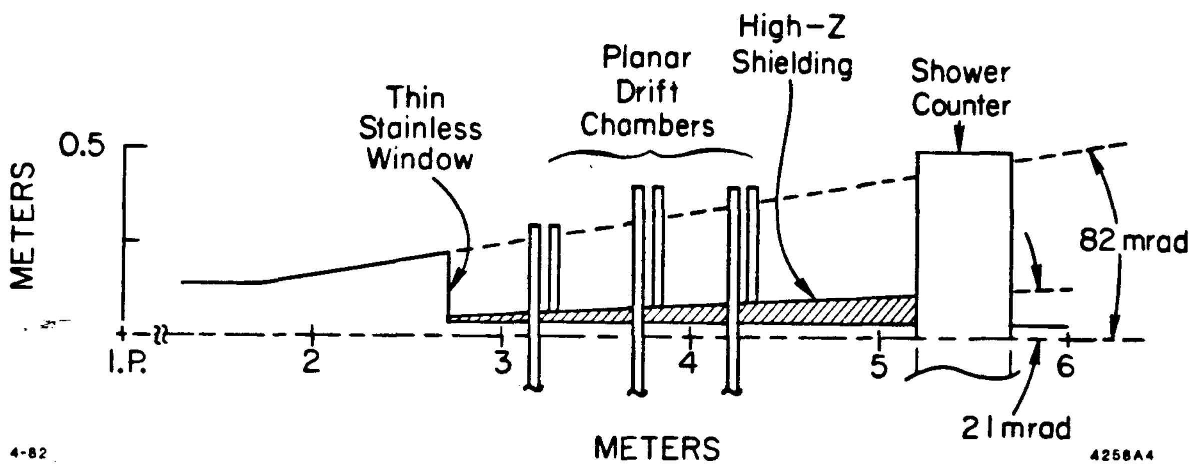
High-Z
Shielding
Planar
Drift
Chambers
Thin
Stainless
Window
Shower
Counter
0.5
METERS
82 mrad
I.P.
2
3
4
5
6
21 mrad
METERS
4-82
4258A4

Fig. 2

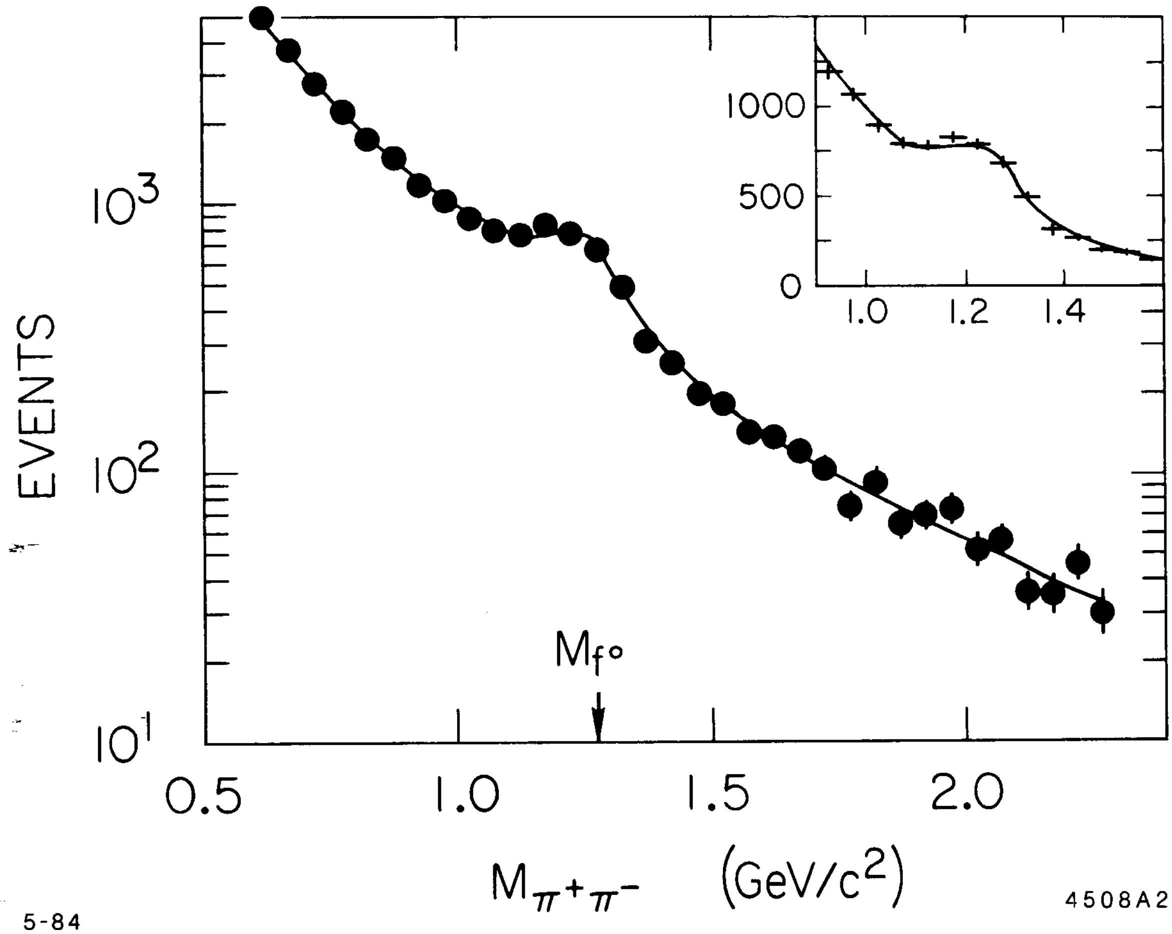

EVENTS
10^3
10^2
10^1
0.5
1.0
1.5
2.0
M_{f°
$M_{\pi^+\pi^-}$ (GeV/c^2)
1000
500
0
1.0
1.2
1.4
5-84
4508A2

Fig. 3

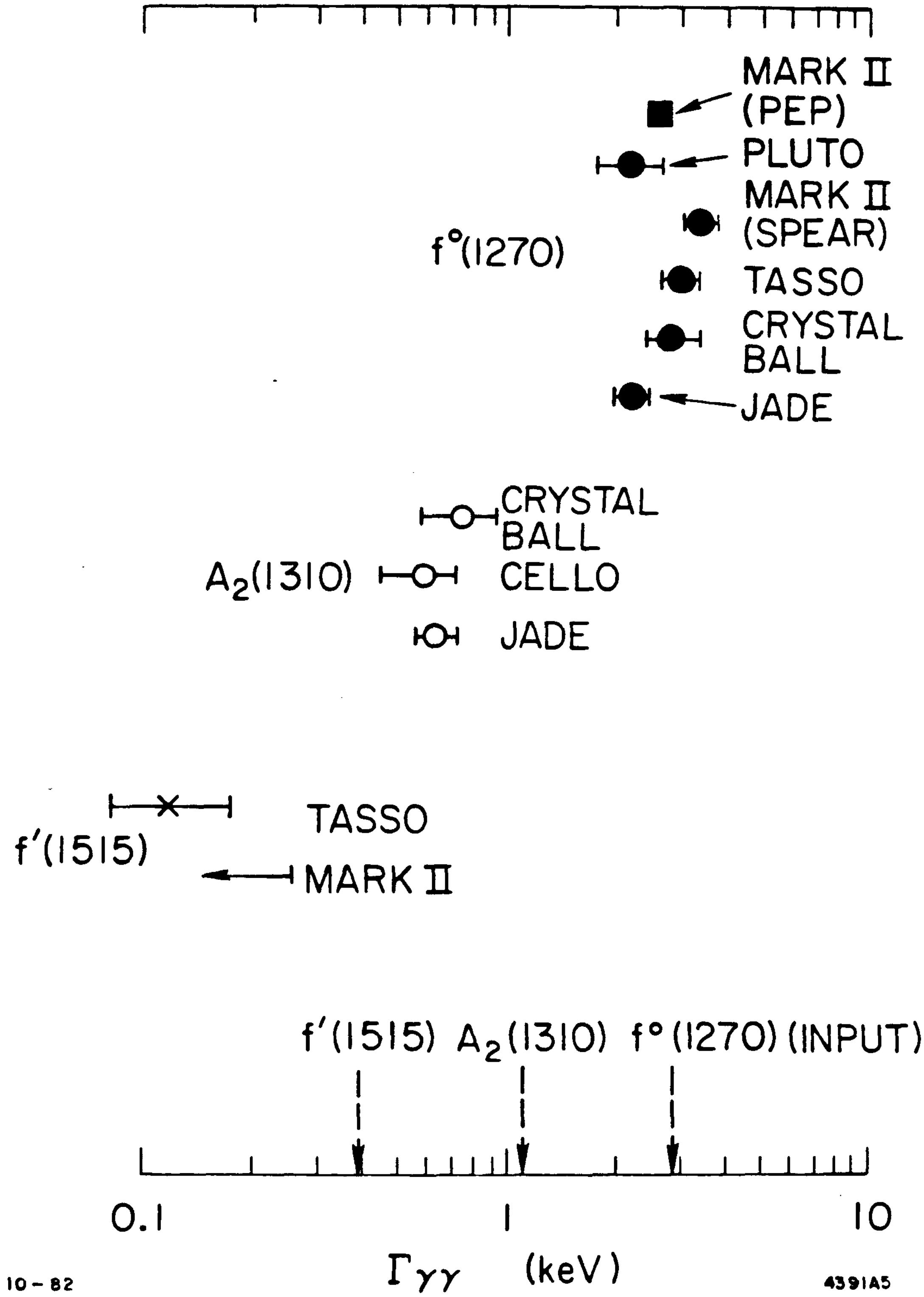
MARK II
(PEP)
PLUTO
MARK II
(SPEAR)
f°(1270)
TASSO
CRYSTAL
BALL
JADE
CRYSTAL
BALL
A2(1310)
CELLO
JADE
TASSO
f′(1515)
MARK II
f′(1515)
A2(1310)
f°(1270) (INPUT)
0.1
1
10
Γγγ (keV)
10-82
4391A5

Fig. 4

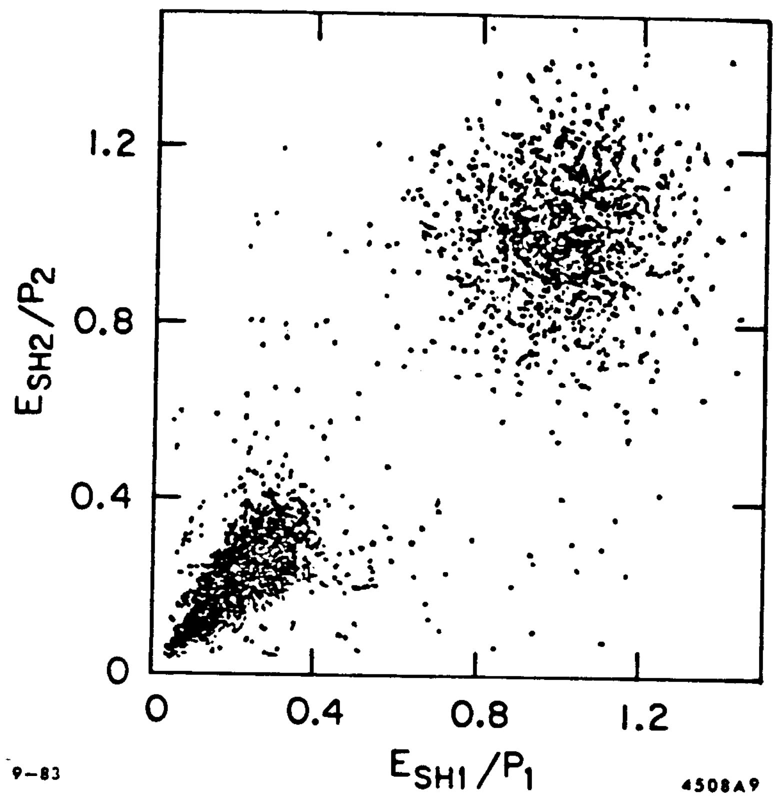

Fig. 5

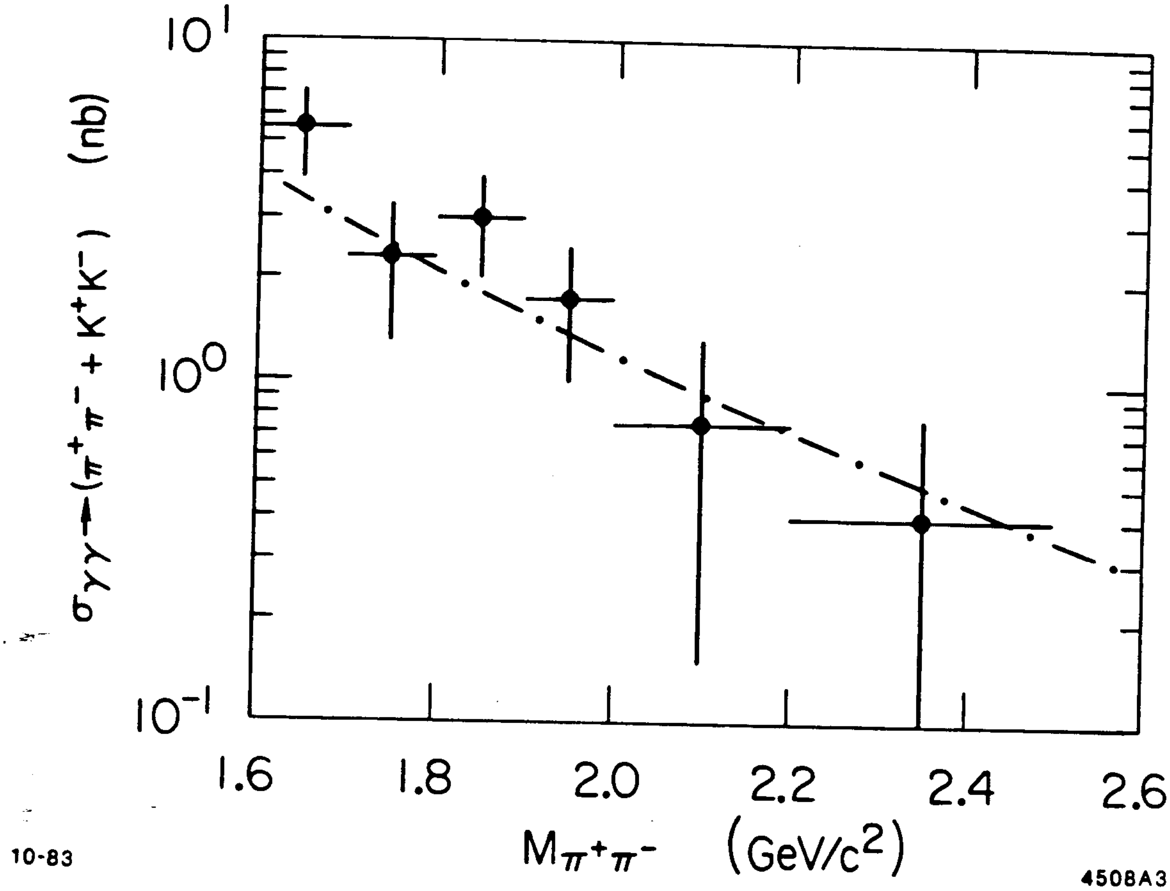
10^1
10^0
10^{-1}
$\sigma_{\gamma\gamma \to (\pi^+\pi^- + K^+K^-)}$ (nb)
1.6
1.8
2.0
2.2
2.4
2.6
$M_{\pi^+\pi^-}$ (GeV/c^2)
10-83
4508A3

Fig. 6

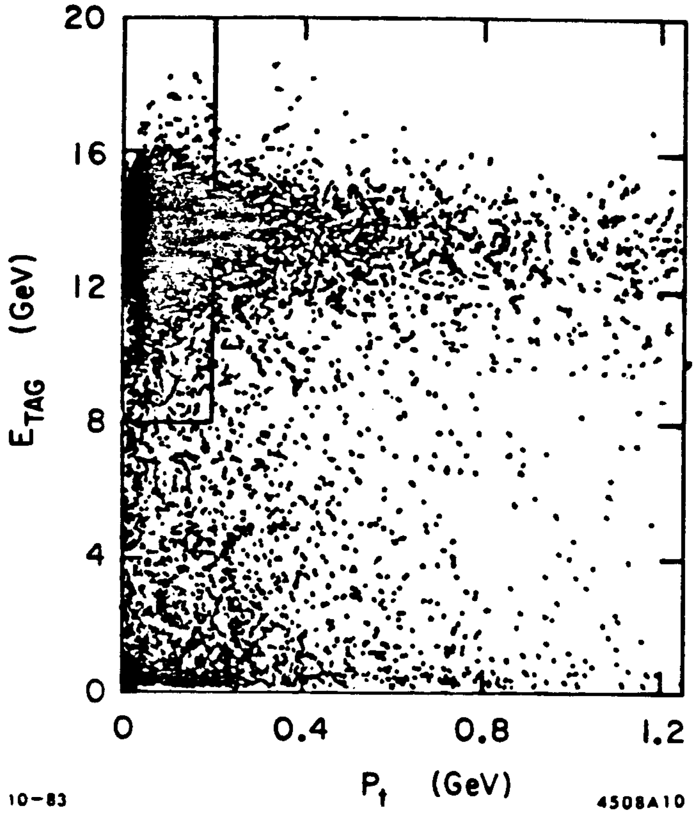

Fig. 7

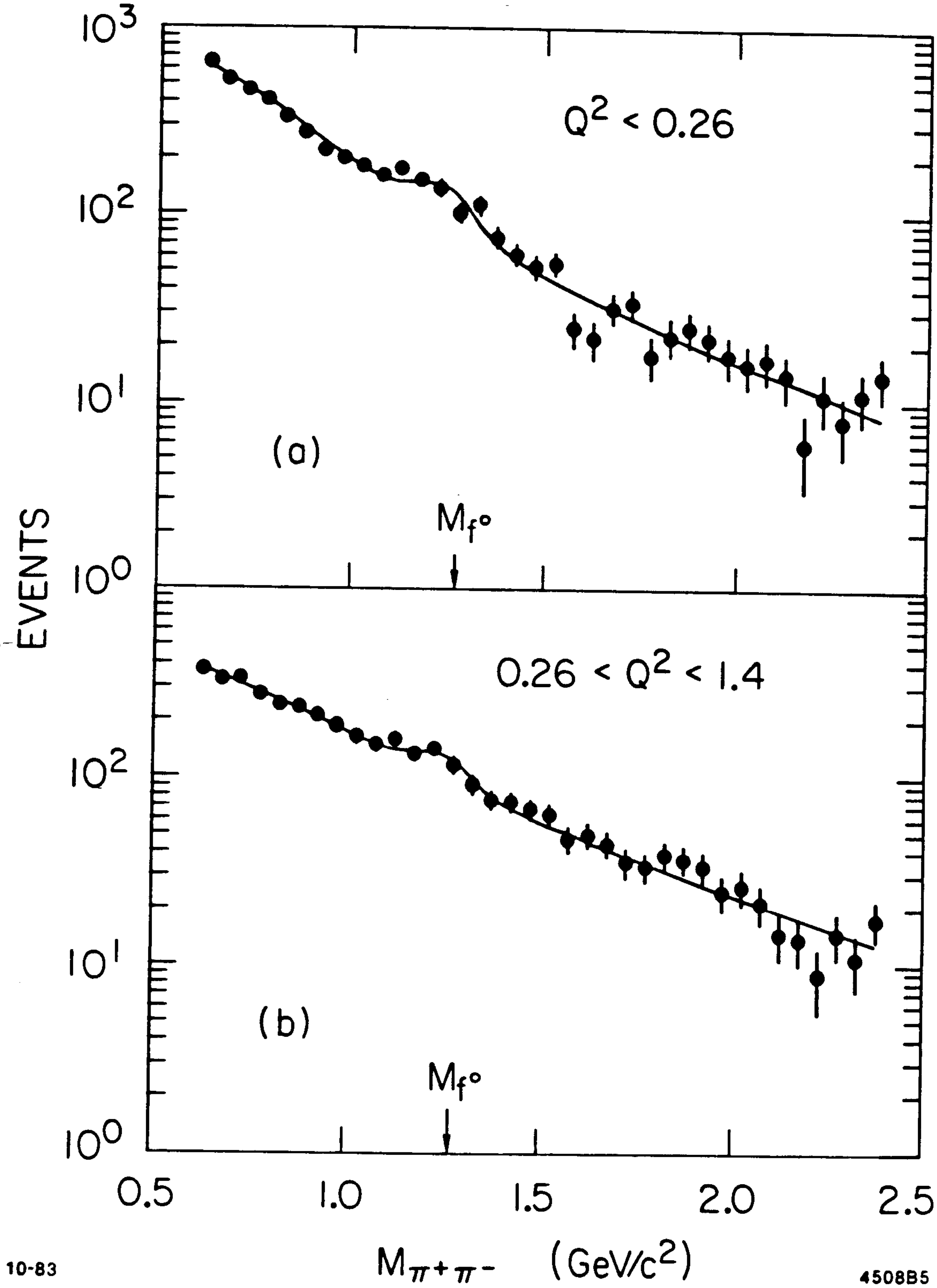

10^3
10^2
10^1
10^0
$Q^2 < 0.26$
(a)
M_{f°
EVENTS
$0.26 < Q^2 < 1.4$
10^2
10^1
10^0
(b)
M_{f°
0.5
1.0
1.5
2.0
2.5
10-83
$M_{\pi^+\pi^-}$ (GeV/c^2)
4508B5

Fig. 8

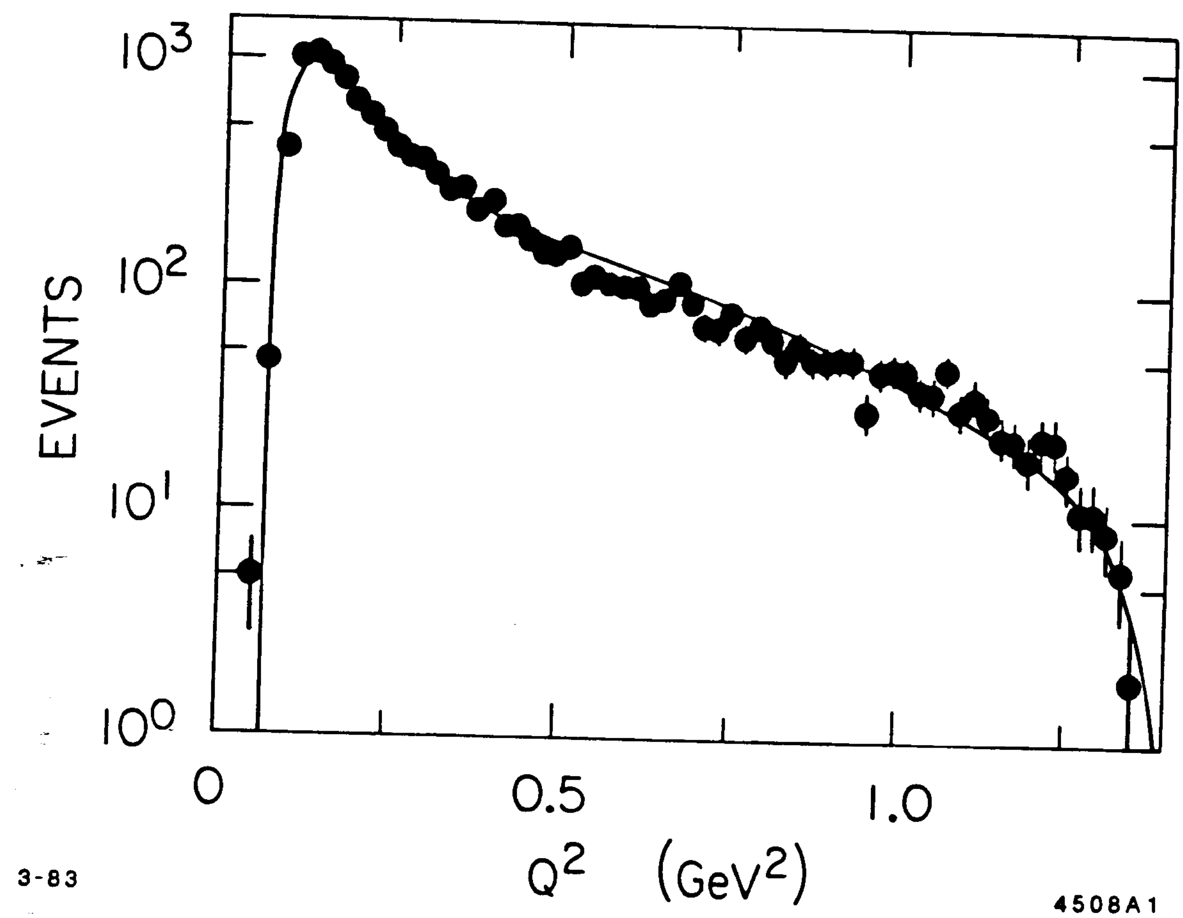

Fig. 9

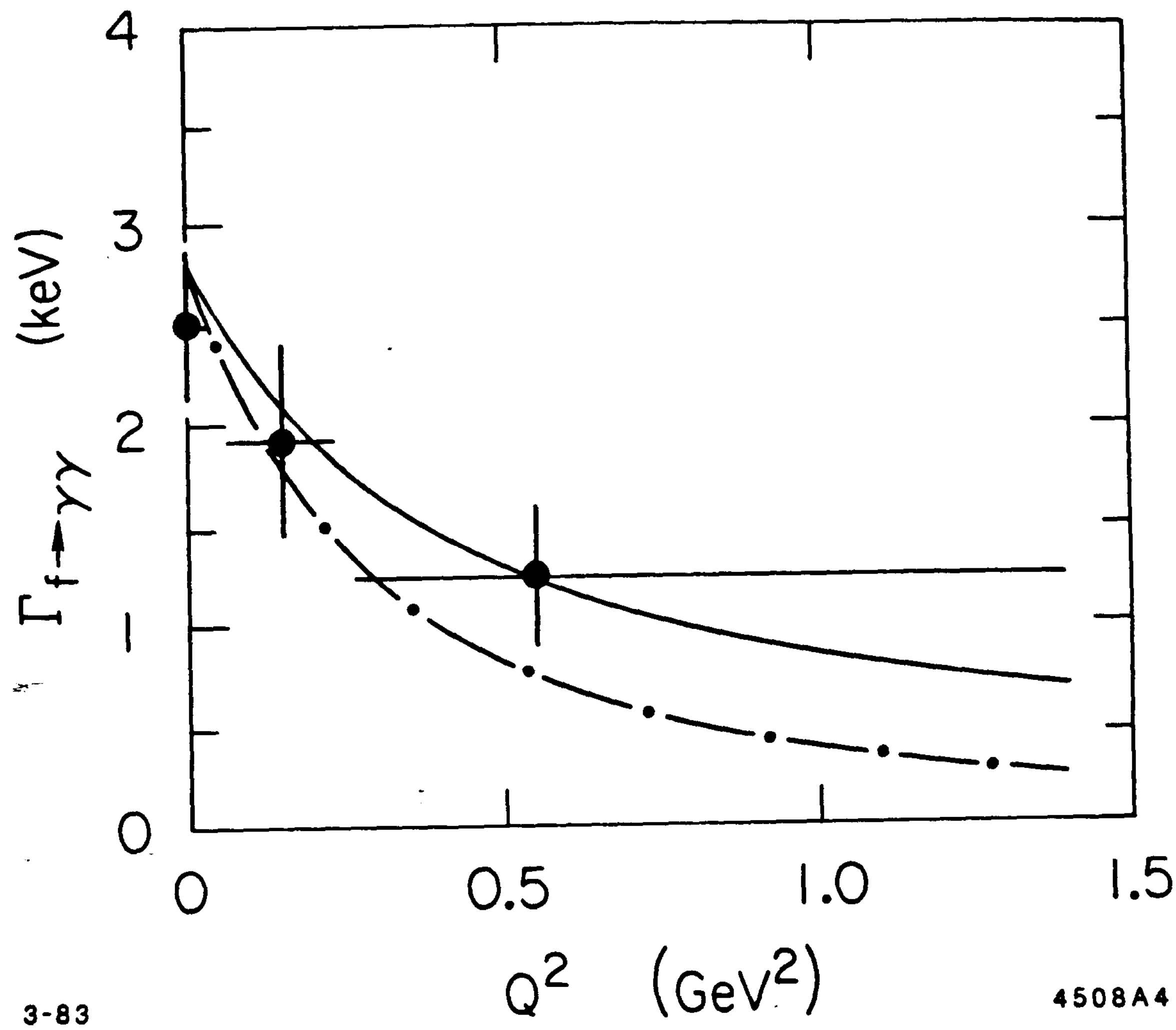

Fig. 10